nature nanotechnology

PERSPECTIVE

https://doi.org/10.1038/s41565-020-0713-6

Check for updates

Towards single-species selectivity of membranes with subnanometre pores

Razi Epsztein[1,2], Ryan M. DuChanois[1], Cody L. Ritt[1], Aleksandr Noy[3,4] and Menachem Elimelech[1]✉

Synthetic membranes with pores at the subnanometre scale are at the core of processes for separating solutes from water, such as water purification and desalination. While these membrane processes have achieved substantial industrial success, the capability of state-of-the-art membranes to selectively separate a single solute from a mixture of solutes is limited. Such high-precision separation would enable fit-for-purpose treatment, improving the sustainability of current water-treatment processes and opening doors for new applications of membrane technologies. Herein, we introduce the challenges of state-of-the-art membranes with subnanometre pores to achieve high selectivity between solutes. We then analyse experimental and theoretical literature to discuss the molecular-level mechanisms that contribute to energy barriers for solute transport through subnanometre pores. We conclude by providing principles and guidelines for designing next-generation single-species selective membranes that are inspired by ion-selective biological channels.

Over the past several decades, reverse osmosis (RO) desalination has become the leading technology for augmenting fresh water supply around the world. The rise of this technology is primarily attributed to the development of a highly permeable thin-film composite (TFC) polyamide membrane with high salt rejection[1]. Extensive research has sought to further increase the water permeability of desalination membranes[2], but it has been shown that greater permeability would only marginally improve the energy efficiency of desalination[3]. This realization initiated a new research thrust aimed at developing membranes with ultra-high water–solute selectivity[4–6]. The primary appeal of ultra-high water–solute selectivity, or solute rejection, is that greater retention of all solutes would ensure higher water quality and avoid costly post-treatment steps[3]. However, to date, these efforts have failed to produce selective layers with higher performance than current TFC polyamide membranes, mainly due to unavoidable defects inherent to the top-down approaches used to fabricate the selective layers[2,4,7,8]. More recently, demand has grown for selective separation of a single solute from water[9–11]. This third research avenue aimed at increasing solute–solute selectivity requires high-precision separation with membranes that can discriminate between different solutes.

Membranes with high solute–solute selectivity would enable more sustainable water-treatment processes. Such membranes could selectively separate problematic contaminants from water and minimize the disposal of concentrated waste streams to the environment. When the end use is drinking water, such fit-for-purpose treatment can also reduce the need for remineralization of product water, thereby reducing treatment cost and use of chemicals[12]. Solute–solute selectivity would also greatly expand the applications of membrane technologies beyond water treatment. Valuable elements, such as lithium or important metals, could be extracted from water at lower chemical and energy consumption compared to existing processes (for example, precipitation, solvent extraction and distillation)[13,14]. Other fields where solute–solute selective membranes could be applied include sensor devices, proton-exchange membranes for fuel cells, and industrial chemical separation processes involving different solvents.

The examples and benefits of high-precision separation discussed above emphasize the paramount importance of a single-species selective membrane. However, conventional membrane fabrication techniques lack the molecular-level design required for achieving solute–solute selectivity. Furthermore, the underlying principles for the design and fabrication of such selective membranes are not well established. Recent advances in ångström-scale fabrication techniques[15,16], combined with insights from nanofluidics and ion-selective biological channels, may provide a gateway to novel, ultra-high solute–solute selective membranes. Translating these advances into the design of multipore membrane systems is critical to realizing the full technological potential of precise solute–solute separations.

In this Perspective, we synthesize experimental and theoretical evidence to provide a design framework for a new class of synthetic membranes with subnanometre pores that are selective for a single species. We first highlight the limitations of conventional membrane materials in achieving solute–solute selectivity. Then, we introduce the transition-state theory to describe energy barriers for solute transport in membranes and discuss the molecular-level mechanisms that can induce selectivity. We conclude by proposing guidelines and new avenues of research for designing novel synthetic membranes with unprecedented solute–solute selectivity.

Existing membranes exhibit limited solute–solute selectivity

Separation technologies based on membranes with subnanometre pores (or free volume elements) can be broadly classified according to the driving force used to induce separation. In RO and nanofiltration (NF) membrane processes (Fig. 1a), an applied hydraulic pressure difference (ΔP) must overcome the osmotic pressure difference ($\Delta\pi$) between the feed and the permeate to drive water through the membrane. Alternatively, forward osmosis (FO) utilizes an osmotic

[1]Department of Chemical and Environmental Engineering, Yale University, New Haven, CT, USA. [2]Faculty of Civil and Environmental Engineering, Technion – Israel Institute of Technology, Haifa, Israel. [3]Materials Science Division, Physical and Life Sciences Directorate, Lawrence Livermore National Laboratory, Livermore, CA, USA. [4]School of Natural Sciences, University of California Merced, Merced, CA, USA. ✉e-mail: menachem.elimelech@yale.edu

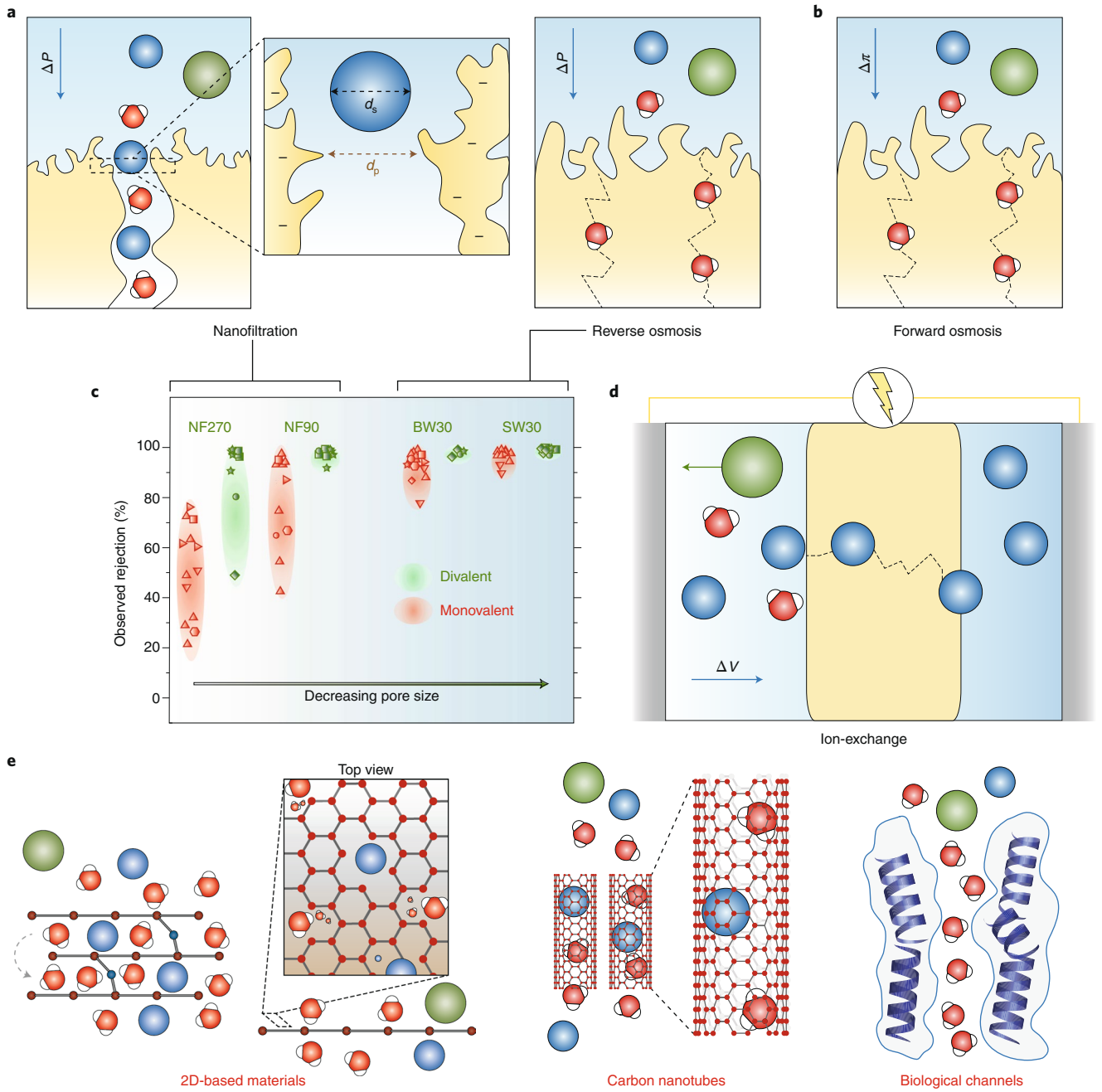

Fig. 1 | Membranes with subnanometre pores. a, Nanofiltration (NF) and reverse osmosis (RO) operate under a hydraulic pressure difference (ΔP). RO membranes significantly hinder the transport of all solutes, whereas NF membranes allow faster permeation of specific solutes (blue spheres) compared to other solutes (green spheres). **b**, Forward osmosis utilizes a concentrated draw solution, creating an osmotic pressure difference ($\Delta\pi$) to drive water across the membrane; solute transport is significantly hindered as in RO. **c**, Observed rejection of various commercial NF (NF270 and NF90, Dow) and RO (BW30 and SW30, Dow) membranes for monovalent (red) and divalent (green) ions in aqueous solution from selected literature[21,22,43,98–113]. NF achieves greater monovalent–divalent ion selectivity than RO due to separating species based on solute properties, such as size and charge. Membrane pore sizes from largest to smallest: NF270, NF90, BW30, SW30. Symbols with different shapes represent various ions. Data were collected under different operating conditions or specified by the manufacturer. **d**, Ion-exchange membranes are used in processes such as electrodialysis that utilizes an electric potential difference (ΔV) and allows passage of counterions (blue spheres) while hindering co-ions (green spheres) and water. **e**, Membranes with subnanometre pores made from novel materials such as 2D nanosheets, aligned single-walled carbon nanotubes or biological channels. 2D-based materials are represented by stacked graphene oxide or reduced graphene oxide with covalent cross-linkers (left) and nanoporous graphene (right).

pressure difference to drive water (Fig. 1b). Achieving solute–solute selectivity with RO and FO membranes is difficult as the dense polymer matrices significantly hinder the transport of most solutes compared to water molecules. Some NF membranes, with slightly larger pores compared to those of RO membranes, can effectively hinder the transport of divalent ions while allowing fast permeation of smaller monovalent ions, thus imparting monovalent–divalent ion selectivity to some extent (Fig. 1c).

Accounting for a small share of the globally desalinated water[17], electrodialysis (ED), an electro-driven membrane process, is used

Box 1 | Transition-state theory for rate processes

In his 1889 work, Arrhenius suggested that an equilibrium exists between inert and active molecules of the reactant during a chemical reaction, where the formation of the active molecules is a crucial step in the conversion process[140]. Based on this idea, he formulated an empirical equation that accounts for the influence of temperature on the specific rate of a chemical reaction:

$$k = A\exp\left(-\frac{E_a}{RT}\right) \quad (1)$$

where k is the specific rate of reaction, T is the absolute temperature, R is the universal gas constant, E_a is the experimental activation energy (that is, the energy that a molecule in the initial state of the process must acquire before it can react) and A is the pre-exponential factor. To apply the Arrhenius equation, it was assumed that both E_a and A can be considered constant within a small temperature range.

The success of the Arrhenius equation to predict the rate of a variety of reactions initiated efforts to explain the equation mechanistically by calculating the rate of a chemical reaction from first principles. In contrast to the empirical evaluation of E_a and A by Arrhenius, first-principle calculations of reaction rates involved the derivation of these parameters utilizing only fundamental properties of the reacting molecules (for example, configurations, dimensions and interatomic forces)[66,141].

Using quantum and statistical mechanics, 'the theory of absolute reaction rates'[66,141], or in its more familiar name 'the transition-state theory' was simultaneously developed by Eyring, Polanyi and Evans and introduced in 1935. The theory assumes that a chemical reaction or other elementary rate process, such as molecular diffusion, is characterized by a continuous change in the configuration of the reactants along the reaction coordinate. The reaction proceeds on the most favourable reaction path (left figure) on the potential-energy surface (a 3D energy profile of the molecule as a function of the position of the atoms) and crosses a critical configuration (the activated complex) situated at the highest point of this path (the saddle point). From this configuration, which is in equilibrium with the reactants, motion in one direction along the reaction coordinate leads to decomposition of the activated complex into a product at a definite rate. With these assumptions, and by knowing the potential energy surface of the system, it is possible to derive the concentration and rate at which the activated complexes pass through the critical configuration of the activated state by statistical methods. The product of these quantities allows the formulation of the specific rate of reaction according to the Eyring equation[66,141]:

$$k = \kappa\frac{k_B T}{h}\exp\left(\frac{\Delta S^{\ddagger}}{R}\right)\exp\left(-\frac{\Delta H^{\ddagger}}{RT}\right) \quad (2)$$

where κ is the transmission coefficient (that is, the ratio of species crossing the barrier to species reaching the barrier, which is taken as unity in many reactions), k_B is the Boltzmann constant, h is the Planck constant, and $\Delta S^{\ddagger}$ and $\Delta H^{\ddagger}$ are the entropy of activation and heat of activation, respectively. While TST generally represents an upper bound for a reaction's rate, several modifications of the Eyring equation have been since formulated to account for deviations from classical mechanics of gas-phase reactions; such modifications typically result in lower predicted rate constants but follow the same temperature dependence[142–145].

Notably, equation (2) provides a molecular-level interpretation for the experimental activation energy (E_a) and pre-exponential factor (A) from the Arrhenius equation in terms of enthalpy and entropy changes, respectively, during the conversion of a reactant molecule into the activated complex. By measuring reaction rates at different temperatures, E_a and A values can be determined experimentally from the slope and intercept, respectively, of the linearized Arrhenius plot (right figure).

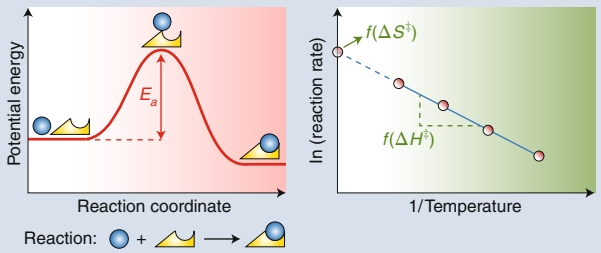

in treating low-salinity waters and other niche applications[18]. In ED, an electric potential difference (ΔV) drives ions across an ion-exchange (IEX) membrane (Fig. 1d). Fixed charged groups in the membrane promote the favourable permeation of oppositely charged counterions while excluding co-ions. However, the ability of IEX membranes to selectively separate between ions possessing the same charge is poor. Notably, ED is limited only to ion separation, as electrically-driven transport does not affect neutral solutes.

Current membrane fabrication techniques, such as interfacial polymerization to fabricate TFC membranes, were developed to improve water–solute selectivity, but they provide limited control over the local structure and chemical nature of membrane pores[2]. Recently, there has been substantial research interest in novel materials, such as two-dimensional (2D) nanosheets, carbon nanotubes (CNTs), and biomimetic channels to address the limitations of current membranes (Fig. 1e)[2]. Such interest in novel materials was sparked by the discovery of exceptional transport characteristics, such as slip flow[19], that could result in membranes with ultra-high water permeability. These novel materials may also provide important features toward solute–solute selectivity such as their structural and chemical homogeneity, as well as facile tunability[19]—features which current membranes lack. However, incorporation of these materials in membranes has been hindered by fabrication-induced defects[2].

Although solute–solute selectivity in state-of-the-art synthetic membranes is relatively limited, consistent selectivity trends are still observed in these membranes due to several transport mechanisms. Notably, these trends manifest more clearly for larger subnanometre pores, such as those in NF and IEX membranes, where the transport of small solutes is less hindered. In order to design membranes with improved solute–solute selectivity, better understanding of the molecular-level mechanisms for solute transport under subnanometre confinement is needed.

Transition-state theory can describe solute transport in membranes

Solute transport through membranes with subnanometre pores can be described as molecular diffusion driven by a chemical potential gradient[20]. Solute–solute selectivity is induced by differences in solute transport rates across the membrane and is commonly evaluated using solute flux or rejection[21–24]. However, to explore solute–solute selectivity beyond measured differences in fluxes and to understand the mechanisms underlying such selectivity, a molecular-level approach to model solute transport is needed.

To diffuse, a solute must successively break bonds with neighbouring molecules in its host medium (for example, water or a membrane pore), advance toward the next coordinate in the medium, and reform stabilizing bonds with its new surroundings. Therefore, molecular diffusion of a solute in a host medium can be considered an elementary reaction and be described using the transition state theory (TST) proposed by Eyring (Box 1)[25–28]. According to this theory, to translocate from one coordinate to the next, a solute must go through an unstable and high-potential energy transition state before establishing new bonds at the next coordinate. This transition state is associated with an energy barrier (also called activation energy), limiting solute transport only to solutes possessing sufficient energy to overcome the energy barrier[29].

Solute transport through the membrane pore can be described as molecular diffusion over multiple barriers in series. Ideally, the solute needs to overcome a single barrier at the pore entrance, cross consecutive barriers inside the pore and then partition back into the solution on the other side of the pore. Assuming such a long diffusion path is governed by a rate-limiting step (that is, partitioning from the bulk solution into the pore or diffusion inside the membrane), the overall transport across the membrane pore can be modelled using single-barrier TST[28]. Hence, an Arrhenius-type equation, similar to Eq. (1) in Box 1, can be applied to describe the solute permeability:

$$P = A' \exp\left(-\frac{E_a}{RT}\right) \quad (3)$$

where P is the solute permeability (the solute flux normalized by the driving force), A' is a pre-exponential factor, E_a is the energy barrier for solute transport, R is the universal gas constant, and T is the absolute temperature. Notably, the Arrhenius behaviour in Eq. (3) is related to intrinsic parameters defining solute permeability such as diffusivity and partition coefficients.

Transition-state theory can elucidate molecular-level phenomena occurring during diffusion through subnanometre pores[30,31]. More specifically, calculation of the energy barrier and the pre-exponential factor from the Arrhenius-type equation (Eq. (3)) can explain the observed solute–solute selectivity in terms of enthalpy and entropy differences between the initial and transition state (Box 1)[32]. In Eq. (3), the pre-exponential factor, A', accounts for the intrinsic frequency at which solute molecules can pass the transition state during diffusion at zero energy barrier (A in Eq. (1)). The energy barrier, E_a, dictates the actual frequency in which solutes can be activated and diffuse across the transition state. Hence, variations in the energy barrier (or pre-exponential factor) between different solutes can induce single-species selectivity (Fig. 2a). Notably, due to the exponential dependence of solute permeability on the energy barrier, a small change in the energy barrier will significantly alter the solute permeability and the resulting selectivity[33].

Molecular-level mechanisms govern energy barriers for solute transport

While the energy barrier for solute transport can be affected by operating conditions (for example, driving force) and solution composition, as well as by interactions with other solutes, solute interactions with the host medium (that is, water and pore walls) provide the most crucial mechanisms to induce solute–solute selectivity. Figure 3a shows examples from selected studies of experimental energy barriers for transport of water and different solutes through membranes and other subnanometre pores. Note that most energy barriers calculated are higher than the activation energy for self-diffusion (or viscosity) of water (~4 kcal mol^{-1})[34], indicating hindered transport. Interpretation of these energy barriers with respect to the different mechanisms that can affect solute–solute selectivity (Fig. 2b) is given below.

The first stage that can impose a significant resistance for solute transport, or an energy barrier, is solute partitioning into the membrane (Fig. 2b, horizontal panel). Size and steric effects (Fig. 2b(i)) are often used to describe solute transport, as they can pose significant energy barriers. For a solute to enter a rigid confined pore with dimensions smaller than its own bare size, reorganization of intramolecular bonds and atoms, or rearrangement of the membrane material, may be necessary. These rearrangements, if feasible at the tested temperature, may result in relatively high energy barriers[35–39](Fig. 3a, ref. [40]).

Electrostatic interactions between solutes and fixed charged groups at the pore mouth (Fig. 2b(ii)) repel co-ions while attracting counterions, thus hindering or promoting solute partitioning, respectively[41,42]. In polymeric NF and IEX membranes, where steric exclusion is not as prominent as in RO membranes, electrostatic effects significantly influence solute transport. Experimental (Fig. 3a, ref. [43]) and simulation studies[44] demonstrate the contribution of electrostatic repulsion to the energy barrier for solute transport through an NF membrane and confined subnanometre pore, respectively. Notably, even like-charge ions can be affected to different extents by the fixed negatively charged carboxyl groups on the polyamide NF membrane pore mouth[43].

The dissociation of salts into ions in solution establishes an electric field, directing the opposite point charge of water molecules toward the ions to reduce the overall electric field formed. This phenomenon leads to the formation of stabilizing hydration shells around the dissolved ions. The ability of water (or any other medium) to dissolve ionized solutes and stabilize them is governed by its dielectric constant[45,46]. The water shell significantly increases the ion size, thus hindering its transport through membranes with pores of similar dimensions. Moreover, the ion solvation shell masks the unique properties of the bare ion, hampering its recognition by the pore, which is essential for differentiation between ions and achieving ion–ion selectivity. However, compared to intramolecular bonds governing steric effects, the bonds between the water shell and the ion are less rigid. Therefore, the water shell is often removed or rearranged when the ion enters a pore smaller than the hydrated ion[44,47–50]. This partial dehydration of ions resulting from dielectric effects (Fig. 2b(iii)) contributes to the energy barrier for ion permeation and can explain, for instance, commonly observed selectivity trends for similar monovalent ions in subnanometre pores. Ions with smaller ionic size, corresponding to higher hydration energy, hold their hydration shell more tightly and therefore experience a higher energy barrier during permeation through polymeric membranes (Fig. 3b,c) and simulated nanopores[48,44].

Dehydration-based energy barriers will manifest at reduced pore size (Fig. 3d) and denser polymeric membranes (Fig. 3b), where the hydrated size of the ion becomes too large to access the pore (Fig. 3e). After partial dehydration and partitioning from one dielectric (the bulk) into another (the pore), dehydrated ions develop interactions with the pore wall which, to some extent, can energetically compensate for the loss (or deformation) of their hydration shell to reduce the energy barrier for partitioning. This phenomenon is well pronounced, for example, in IEX membranes, where attractive interactions between the ion and oppositely charged groups in the polymer matrix compensate for the loss of the hydration shell of the ion and facilitate its transport[23,51]. These compensatory interactions of the ion with the pore material are ion-specific and, perhaps, one of the key components to obtaining single-species selectivity, as we discuss in the next section.

Solute–medium interactions are not limited to ions; they can also be attributed to relatively weak van der Waals (vdW) forces between uncharged solutes and a polarizable pore material (Fig. 2b(iv))[52]. The energy barrier of partitioning for uncharged solutes is ascribed to the energetic cost of breaking relatively weak solute–water bonds and the ability to stabilize the solute within the pore

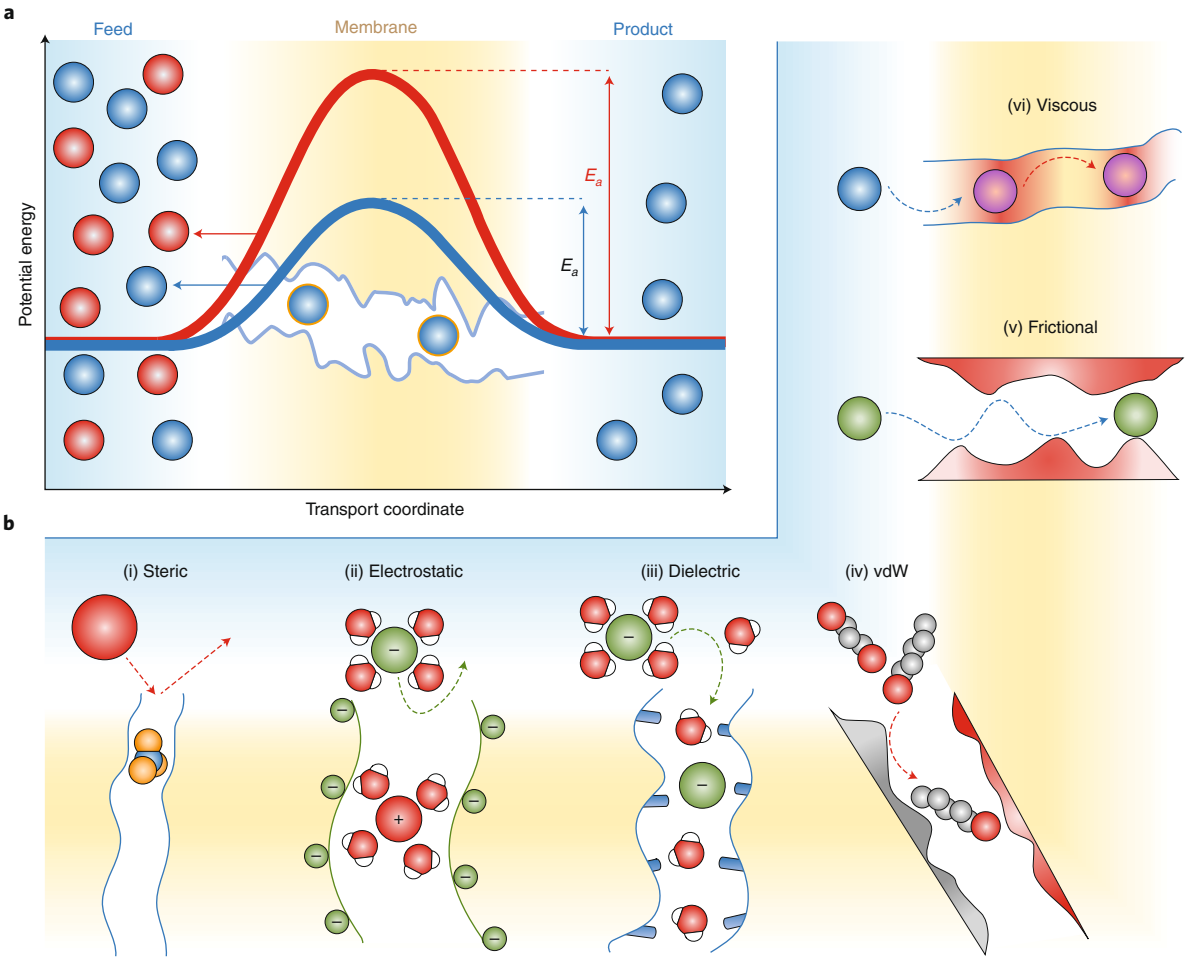

Fig. 2 | Energy barriers for solute transport through membranes with subnanometre pores. a, Energy barrier profiles for two different species (blue and red spheres) transported through a selective membrane. The membrane is permeable only for the blue solute, showing a lower energy barrier (E_a) compared to the red solute. **b**, Mechanisms affecting the energy barrier for solute transport as a result of different elementary reactions. During the partitioning from bulk water into the confined environment of the membrane (horizontal panel), solutes face an energy barrier due to steric hindrance (i) imposed by their size and shape, electrostatic repulsion (ii), dielectric effects (that is, variation in ion interaction with its closest vicinity, such as partial dehydration) (iii) and weak van der Waals (vdW) forces (iv). Solutes experience additional energy barriers while diffusing through the membrane pore (vertical panel) due to frictional (for example, due to physical collisions with rough inner pore walls) (v) and viscous effects (due to the breaking and formation of chemical bonds with the pore wall) (vi). Overall, partitioning into the pore and diffusion in the pore channel can be viewed as two transport resistances that are connected in series.

via interactions with the pore material. For example, energy barriers calculated for the permeation of neutral alcohols with hydrophobic and hydrophilic end groups into biological lipid membranes suggest that the solutes enter the membrane in a fully dehydrated form[53]. In this case, unlike in relatively hydrophilic synthetic polymeric membranes, dehydration is also promoted by the unfavourable interactions between water molecules and the hydrophobic lipid. Reduced energy barriers for glycol, which has a nonpolar methyl end group, were attributed to its ability to develop favourable compensatory interactions with the hydrophobic membrane core.

After a solute partitions into the membrane, its confined diffusion inside the pore is governed by several consecutive barriers that hinder its transport. These barriers originate from solute-specific frictional and viscous interactions with the membrane material (Fig. 2b, vertical panel). Frictional effects (Fig. 2b(v)) stem from physical collisions between solutes and rough surfaces, resulting in momentum exchange, reduced solute kinetic energy and increased energy barrier[54]. On the other hand, viscous (or adhesive) effects (Fig. 2b(vi)) are due to the chemical affinity of a solute to the pore wall[26]. This affinity is dictated by the extent of attractive interactions (for example, vdW and electrostatic) between the solute and the pore wall. Higher solute affinities to the pore material lead to higher energy barriers that must be overcome for a solute to translocate to the next coordinate in the pore. These viscous effects during hindered solute diffusion may counteract solute partitioning into the pore; that is, higher solute affinity to the pore material will promote partitioning into the pore but hinder diffusion inside the pore, and vice versa. Therefore, the observed selectivity depends on the relative contribution of solute partitioning into the pore and its diffusion inside the pore to the overall energy barrier.

Biological channels provide guidelines for ultra-high solute–solute selectivity

Improvement of solute–solute selectivity in state-of-the-art synthetic membranes is often pursued by modification of membrane charge[22,24], variation of pore size[55,56], incorporation of specific chemical functionality[57,58], and adjustment of operating (or solution) conditions[24,41,59]. While partial successes have been reported,

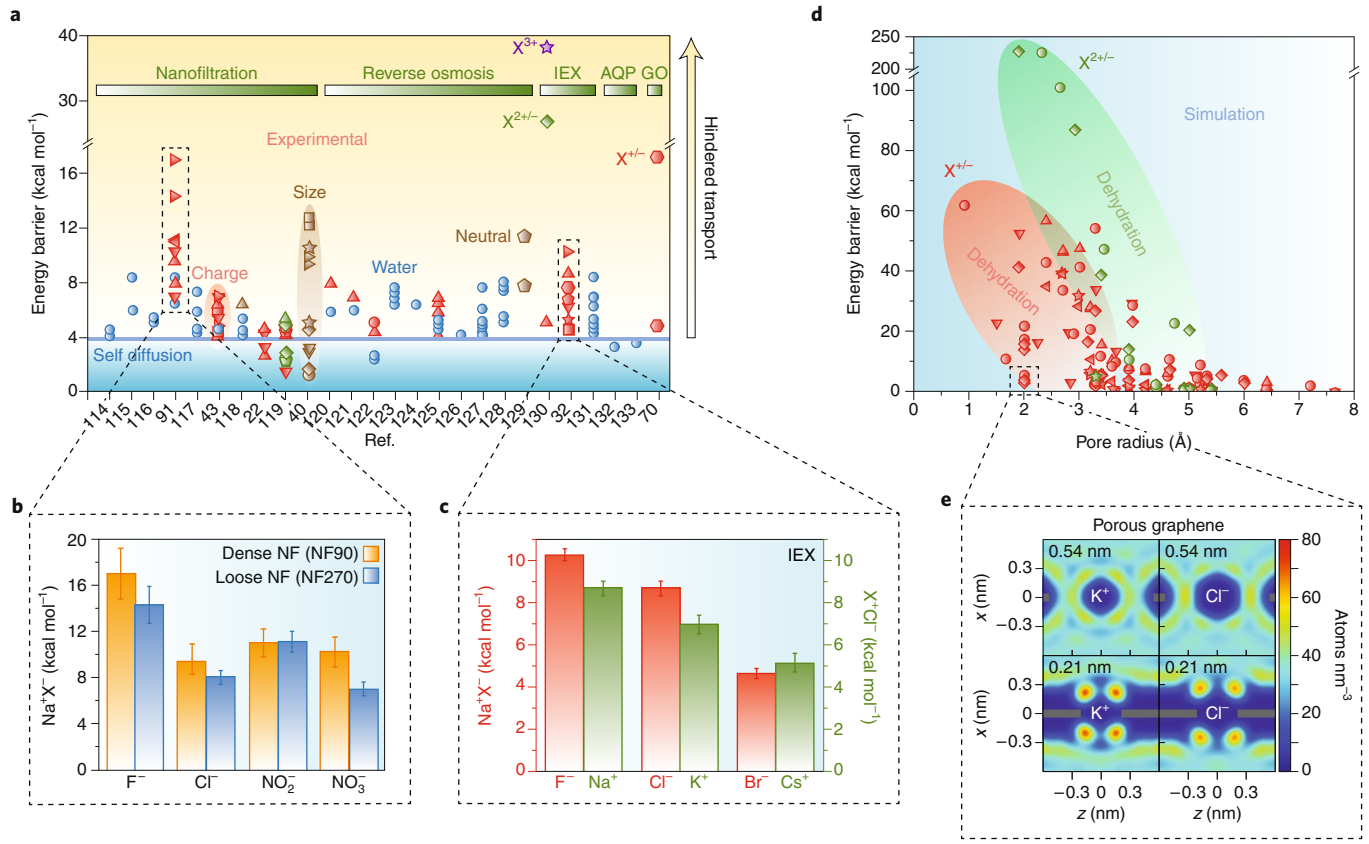

Fig. 3 | Experimental and simulated energy barriers for water and solute transport through different subnanometre pores. a, Experimental energy barriers calculated using an Arrhenius-type equation (Eq. (3)) by measuring solute permeability at different temperatures for nanofiltration (NF)[22,40,43,91,114–119], reverse osmosis (RO)[120–129] and ion-exchange (IEX) membranes[32,130,131], as well as aquaporin (AQP) water channels[132,133] and graphene oxide (GO) membranes[70]. Numbers on the horizontal axis represent different literature references. Solute transport is considered hindered when its energy barrier is higher than the energy barrier for self-diffusion (or viscosity) of water (blue borderline, ~4 kcal mol^{-1})[34]. Blue, brown, red, green and purple symbols represent water, neutral solutes, monovalent ions, divalent ions and trivalent ions, respectively. Activation energies for all ions were measured for salts containing the relevant ion and a counterion. Symbols of different shapes represent various solutes. **b**,**c**, Experimental energy barriers from ref. [91] and ref. [32], respectively, indicating partial dehydration of monovalent ions at the pore entrance of NF and IEX membranes, respectively. Partial dehydration of ions is governed by ion hydration energy and membrane pore size. **d**, Energy barriers calculated using molecular dynamics simulation for carbon nanotubes[134,135], graphene oxide membranes[70,136], porous graphene[47,137,138] and other hydrophobic pores[44,48,49,139] of different pore radii. Monovalent (red symbols) and divalent (green symbols) ions undergo partial dehydration at the pore entrance as pore size decreases, resulting in an increased energy barrier. Symbols of different shapes represent various solutes. In **a**–**d**, X represents different anions and cations. **e**, Partial dehydration demonstrated using oxygen density simulation for water around a K^+ or Cl^- ion fixed at the centre of a 2.1 Å or 5.4 Å pore (grey) in a graphene sheet. For the 2.1 Å pore, the first hydration shell is distorted by the pore edge. The horizontal and vertical coordinates are represented by *z* and *x*, respectively. Panel **e** adapted with permission from ref. [47], American Chemical Society.

the selectivity obtained is usually not solute specific and is limited to a group of solutes possessing a certain property, such as divalent cations (Fig. 1c). Therefore, a more holistic approach with a set of rules and principles should be applied for designing a single-species selective membrane (Fig. 4a).

Biological ion channels provide an inspirational glimpse into ideal single-species selectivity. Extensive work by MacKinnon[60–62] elucidated the architecture and working mechanism of the K^+ channel, which can transport K^+ ions 10,000 times faster than Na^+ ions through the cell membrane to enable fundamental cellular processes (Fig. 4b). Ultra-selective and fast K^+ conduction is possible due to the combination of several features and physical principles that are discussed below. These principles also underlie the selectivity in other ion-selective biological channels[63], providing guidelines for future membrane design. Although mimicking the precision of nature poses a daunting challenge[64,65], most of the key principles provided below can be applied with existing and emerging fabrication techniques, and preliminary success has already been demonstrated, as discussed in the next section.

Analysis of the K^+ channel reveals a selectivity filter as short as 12 Å, approximately a quarter of the entire length of the channel spanning the lipid bilayer[61]. This ultra-thin layer is optimal to discriminate between solutes by imposing different energy barriers for their transport (Fig. 4c(i)). A longer selectivity filter with high affinity for the target solute (and low affinity for other solutes) could result in higher transport hindrance of the target solute compared to other solutes, thus reducing selectivity. This counteracting effect is well evidenced in micrometre-thick IEX membranes, where the observed selectivity is induced by ion adsorption (or partitioning), but impaired by ion diffusion in the thick membrane[32]. However, because solute permeability is inversely dependent on both the energy barrier and membrane thickness[28], an extremely thin selective layer may result in higher permeation of undesired solutes (Fig. 4c(ii)).

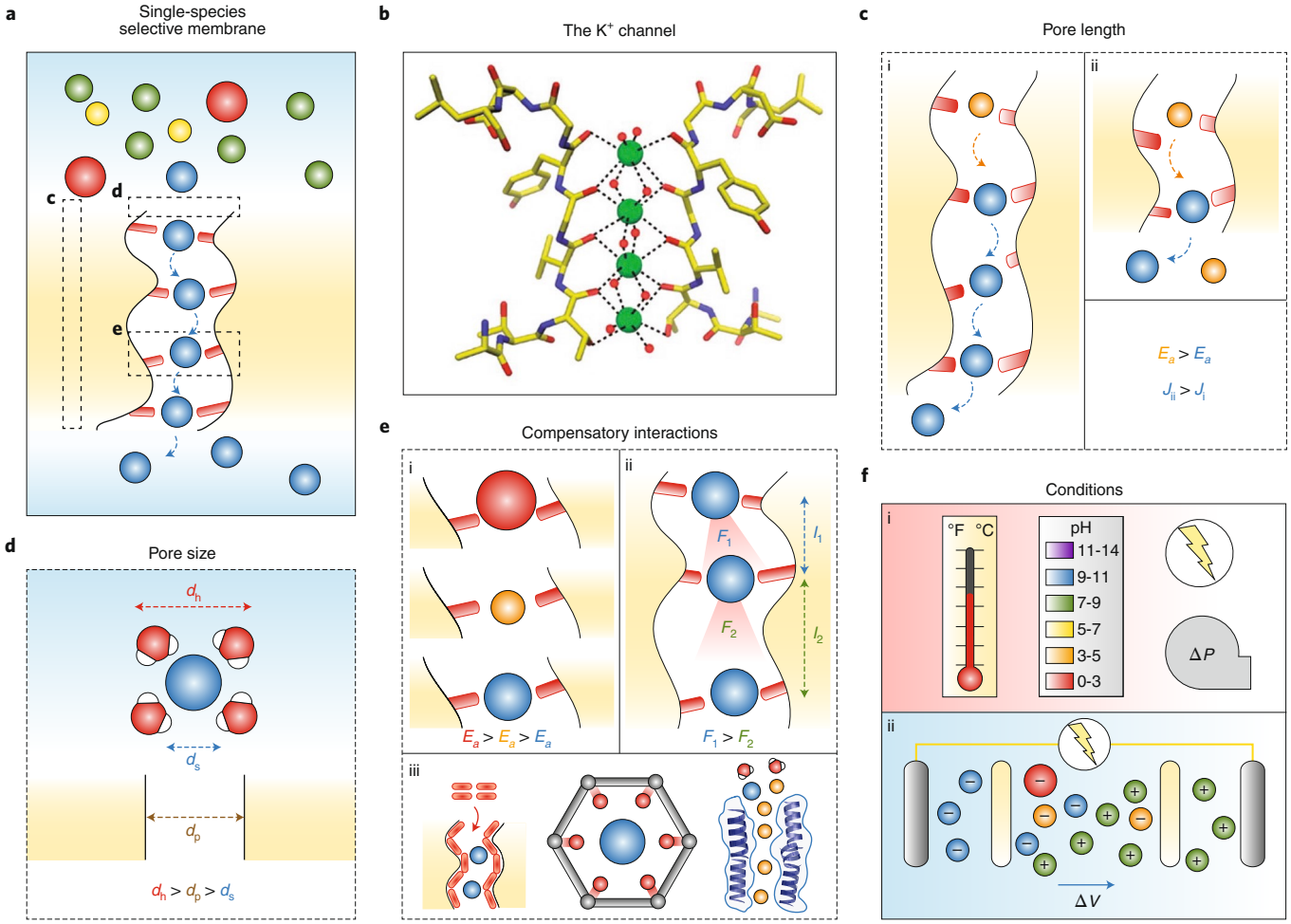

Fig. 4 | Guidelines for designing single-species selective membranes. a, A single-species selective membrane that transfers only blue solutes. Grey dashed boxes refer to membrane properties discussed in **c**–**e**. **b**, The selectivity filter of the biological K^+ channel. The dehydrated K^+ ion (green sphere) fits perfectly in the binding site and interacts with the partial-charge-bearing oxygen groups on the filter (red rods) that serve as surrogates for water molecules **c**, Pore length should be optimized. An optimized pore length is short enough to allow high flux (J) of the target solute (blue sphere), while still preventing other solutes (yellow sphere) from penetrating (i). In a very short pore, undesired species with higher energy barrier (E_a) than the target solute can penetrate (ii). **d**, The pore size (d_p) should be smaller than the solute hydrated size (d_h) but larger than the bare solute size (d_s) to induce dehydration and allow recognition of the right species. **e**, Binding sites along the pore can provide compensatory interactions with the dehydrated species. The cavity size should perfectly match the dehydrated species size to reduce the energy barrier of transport (i). To facilitate the release of the target species from its binding site, a new species should approach and exert a repulsive force (ii). Closely spaced binding sites will exert greater force (F_1) than far-spaced sites (F_2), resulting in a decreased energy barrier for transport. The distances between adjacent binding sites are denoted as l_1 and l_2. Coordination chemistry and advanced fabrication techniques can be applied to stabilize solutes (iii). Shown are atomic layer deposition (iii, left), ionophores (iii, middle) and biological channels (iii, right). **f**, Conditions during separation can alter intrinsic properties of the involved species and membrane and affect the separation (i). To enable separation of a single ion (blue anion) from like-charge ions (red and orange anions), interfering oppositely charged ions (green cations) should be transported through another membrane utilizing an electric potential gradient (ΔV) (ii). Panel **b** reproduced with permission from ref. [63], AAAS.

For the selectivity filter to recognize the correct solute in a multi-species solution, solutes need to shed their hydration shell to expose their unique properties (for example, non-hydrated size and charge). To induce solute dehydration, a pore size (d_p) smaller than the size of the hydrated solute (d_h) should be designed (Fig. 4d); however, the pore size must be larger than the size of the non-hydrated solute (d_s) to reduce steric effects (Fig. 2b(i)) and allow solute permeation. As solute hydrated size can be significantly larger than its non-hydrated size[45], the required pore size range ($d_h > d_p > d_s$) is relatively large and can be practically tuned for polymeric membranes and other subnanometre pores using existing fabrication techniques.

Following solute dehydration, the key features for selectivity are the compensatory interactions provided by functional groups or binding sites at the pore wall that serve as surrogate water and stabilize the target solute (Fig. 4e)[63]. In the K^+ channel, ultra-selective K^+ conduction is possible due to proper steric and electrostatic containment of dehydrated K^+ within specific binding sites along the selectivity filter[61]. Dehydrated Na^+ ions are too small for these binding sites, which can favourably interact only with dehydrated K^+. These interactions compensate for the energetic cost of K^+ dehydration, stabilize it and reduce the energy barrier of its permeation (Fig. 4e(i)). According to TST (Box 1)[66,67], these binding sites can be viewed as a catalyst that permits transport via a path with lower energy of activation. Another substantial feature of the selectivity filter is the relatively short distance between two binding sites, which generates mutual repulsive forces between adjacently bound K^+ ions (Fig. 4e(ii)). This mutual repulsive force assists in

overcoming attractive forces between the K^+ ions and the selectivity filter, reducing the energy barrier of K^+ permeation and maintaining its high conduction[61,68].

Novel fabrication techniques offer pathways for selective membranes

Engineering pores with compensatory interactions that can selectively stabilize a target solute (Fig. 4e(iii)) is highly challenging. One of the major difficulties is the upscaling of pores designed on the molecular level into a defect-free multipore system. In addition, tuning conventional membrane materials (Fig. 1a–d) for such a purpose is impractical due to their inherent chemical heterogeneity as well as surface roughness that exceeds the ångström-scale precision required for high solute–solute selectivity[69]. Instead, membranes from advanced materials with atomically tunable dimensions as well as homogeneous smooth surfaces (Fig. 1e) create opportunities to mimic molecular phenomena in biological channels. Specifically, such materials can induce solute dehydration by their small pore size and subsequently stabilize a solute by perfect containment and interaction with the pore wall.

Extensive research has been devoted to tuning the interlayer spacing in graphene oxide membranes under wetting[70–74]. Functionalized subnanometre carbon nanotubes can also serve as a platform for selective separation[75,76]. Here, besides tuning pore diameter, major challenges include functionalization of the pore interior without compromising structural features, and incorporation and alignment of the tubes in an impermeable matrix[75,77]. While major research efforts with these materials were directed to improving water–solute selectivity and desalination performance, intriguing separations between solutes have also been reported[70,76], calling for future research using these tunable materials to study and improve solute–solute selectivity. Atomic layer deposition (ALD) of small precursors, such as SiO_2 and TiO_2, in cylindrical nanopores is another potential tool to reduce pore size to molecular dimensions and adjust functionality with atomic precision (Fig. 4e(iii), left)[78,79].

Coordination chemistry, where receptors bind specific species to form a host–guest complex, is another avenue to pursue selective in-pore solute stabilization (Fig. 4e(iii), middle). Such molecular recognition between the host and guest molecules depends on molecular topology, dimensionality and coordination number (that is, number of bonds available between the guest and host molecule)[80]. While ionophores naturally occur in biological systems to facilitate transport of specific solutes across lipid membranes (Fig. 4e(iii), right)[81], a large body of research has focused on developing synthetic macrocyclic and macromolecular receptors[82–84]. Traditionally, these receptors have been mostly used as mobile carriers in liquid and polymer-inclusion membranes for sensing[85] and extracting[86] different ions and molecules. More recently, the feasibility of facilitated transport using coordination chemistry was demonstrated for solute–solute separation in subnanometre polymeric membranes[87,88], metal–organic framework channels[10,11], solid-state nanopores[89], and strain-tuned crown ether nanopores in graphene[90].

Operating and solution conditions impact solute–solute selectivity

Apart from membrane structure and chemistry, operating conditions (such as driving force) and solution chemistry can also affect the separation efficiency (Fig. 4f(i)). Solution pH, for instance, strongly influences both solute and membrane charge[41,43,42], affecting both the electrostatic- (Fig. 2b(ii)) and dielectric-based (Fig. 2b(iii)) energy barriers for solute permeation[44]. Operating at elevated chemical potential (for example, high solute concentration) can increase the potential energy of undesired solutes in the feed solution, assisting them in permeating the membrane and impairing selectivity[91,92]. High salt concentration was also shown to promote ion pairing, which lowers the energy barrier for salt permeation through lipid membranes[93].

The type of driving force applied can also affect ion–ion selectivity due to charge balance considerations. The K^+ channel, similar to other single-species biological channels, transports a single type of ion[61]. However, for electroneutrality to be conserved, co-transport of an ion with opposite charge or a counter-transport of an ion with the same charge must occur simultaneously through other channels. Electro-driven processes such as ED inherently separate charge by transporting anions and cations thorough anion- and cation-exchange membranes, respectively. This form of operation provides a platform for engineering a set of single-counterion selective IEX membranes (Fig. 4f(ii))[32]. In contrast, achieving single-ion selectivity in pressure-driven processes such as NF is impossible due to the interlinked transport of anions, cations and water. In this case, single-species selective pores—instead of single-species selective membranes—can theoretically be used in mosaic membrane architectures, which contain more than one type of pore (for example, separate pores for anions and cations)[94,95].

Perspectives and outlook

In light of the limited ability of current membranes with subnanometre pores to meet the growing demand for fit-for-purpose applications, it is imperative to develop a new class of membranes that can effectively discriminate between solutes. Such solute–solute selectivity is based on several molecular-scale features that are absent in state-of-the-art membranes such as NF, RO and IEX. Extensive research on ion-selective biological channels, together with more recent molecular simulation studies, have elucidated the general principles for the design of single-species selective membranes. Future efforts should aim at deeper understanding of such principles at the molecular level and incorporating them into multipore membrane systems.

The molecular basis for solute–solute selectivity in synthetic membranes is not fully understood, mainly due to lack of experimental techniques with the required spatial and temporal resolution to study the kinetics of solute transport within pores. Molecular simulations are a powerful tool to gain mechanistic understanding of solute transport (for example, partial dehydration at the pore mouth), addressing some of our knowledge gaps of solute–solute selectivity. However, a full and unbiased tracking of molecular transport through a long membrane pore is challenging to achieve due to computational limitations of simulating the large time scales of solute transport[96] as well as the chemical heterogeneity of polymeric membranes. Recently developed advanced sampling techniques[96,97] provide an opportunity to study the kinetics of solute transport in long pores to better understand the molecular origin of selectivity and establish structure-selectivity relationships that are essential for the development of membranes with single-species selectivity.

The conventional solution-diffusion model, frequently used to describe transport in dense polymeric membranes such as RO, is limited in explaining molecular-level phenomena that govern water and solute permeation. Instead, the transition-state theory, which is seldom utilized to describe transport in membranes, can experimentally delineate mechanisms governing solute–solute selectivity by providing molecular interpretation for enthalpy and entropy changes that occur during solute transport. Notably, experimental energy barriers and pre-exponential factors serve as an important bridge for concurrent simulation studies on molecular transport in subnanometre pores.

Single channels from novel materials with well-defined geometry and chemistry open opportunities to unravel detailed mechanisms of solute transport. In long and heterogeneous pores of multipore membrane systems, the relative contribution of each hindrance mechanism for solute transport is poorly understood and cannot be properly distinguished. Using emerging techniques to fabricate

channels with precise and known structure, it is possible to systematically simulate each distinct hindrance mechanism and probe its effect on solute–solute selectivity.

In addition to understanding the mechanisms for selectivity, ongoing advances in membrane fabrication techniques are essential for the design of single-species selective membranes. We envision two parallel avenues to fabricate single-species selective membranes with currently available techniques. Incorporation of selective receptors into polymeric membranes has shown some preliminary success[87]. Here, the goal is to achieve fast conductance of the bound target solutes between fixed receptors and minimum penetration of undesired species. Simultaneously, current efforts to accurately tune pore size and chemical functionality of novel materials, such as 2D graphene sheets and carbon nanotubes, should seek to enhance solute–solute separation in addition to water–solute selectivity. In both avenues, incorporation of these novel pore architectures into homogenous and defect-free multipore systems will be the key next step for the implementation of single-species selective membranes.

Received: 17 October 2019; Accepted: 12 May 2020;
Published online: 12 June 2020

References

1. Elimelech, M. & Phillip, W. A. The future of seawater desalination: energy, technology, and the environment. *Science* **333**, 712–717 (2011).
2. Werber, J. R., Osuji, C. O. & Elimelech, M. Materials for next-generation desalination and water purification membranes. *Nat. Rev. Mater.* **1**, 1–15 (2016).
3. Werber, J. R., Deshmukh, A. & Elimelech, M. The critical need for increased selectivity, not increased water permeability, for desalination membranes. *Environ. Sci. Technol. Lett.* **3**, 112–120 (2016).
4. Park, H. B., Kamcev, J., Robeson, L. M., Elimelech, M. & Freeman, B. D. Maximizing the right stuff: The trade-off between membrane permeability and selectivity. *Science* **356**, 1138–1148 (2017).
5. Werber, J. R. & Elimelech, M. Permselectivity limits of biomimetic desalination membranes. *Sci. Adv.* **4**, eaar8266 (2018).
6. Werber, J. R., Porter, C. J. & Elimelech, M. A path to ultraselectivity: Support layer properties to maximize performance of biomimetic desalination membranes. *Environ. Sci. Technol.* **52**, 10737–10747 (2018).
7. Ritt, C. L., Werber, J. R., Deshmukh, A. & Elimelech, M. Monte carlo simulations of framework defects in layered two-dimensional nanomaterial desalination membranes: implications for permeability and selectivity. *Environ. Sci. Technol.* **53**, 6214–6224 (2019).
8. Homaeigohar, S. & Elbahri, M. Graphene membranes for water desalination. *NPG Asia Mater.* **9**, e427 (2017).
9. Luo, T., Abdu, S. & Wessling, M. Selectivity of ion exchange membranes: A review. *J. Memb. Sci.* **555**, 429–454 (2018).
10. Zhang, H. et al. Ultrafast selective transport of alkali metal ions in metal organic frameworks with subnanometer pores. *Sci. Adv.* **4**, eaaq0066 (2018).
11. Li, X. et al. Fast and selective fluoride ion conduction in sub-1-nanometer metal-organic framework channels. *Nat. Commun.* **10**, 2490 (2019).
12. Alvarez, P. J. J., Chan, C. K., Elimelech, M., Halas, N. J. & Villagrán, D. Emerging opportunities for nanotechnology to enhance water security. *Nat. Nanotechnol.* **13**, 634–641 (2018).
13. Sadeghi, I., Kaner, P. & Asatekin, A. Controlling and expanding the selectivity of filtration membranes. *Chem. Mater.* **21**, 7328–7354 (2018).
14. Nghiem, L. D. et al. Extraction and transport of metal ions and small organic compounds using polymer inclusion membranes (PIMs). *J. Memb. Sci.* **281**, 7–41 (2006).
15. Thiruraman, J. P. et al. Angstrom-size defect creation and ionic transport through pores in single-layer MoS_2. *Nano Lett.* **18**, 1651–1659 (2018).
16. Radha, B. et al. Molecular transport through capillaries made with atomic-scale precision. *Nature* **538**, 222–225 (2016).
17. Jones, E., Qadir, M., van Vliet, M. T. H., Smakhtin, V. & Kang, S. The state of desalination and brine production: A global outlook. *Sci. Total Environ.* **657**, 1343–1356 (2019).
18. Campione, A. et al. Electrodialysis for water desalination: A critical assessment of recent developments on process fundamentals, models and applications. *Desalination* **434**, 121–160 (2018).
19. Faucher, S. et al. Critical knowledge gaps in mass transport through single-digit nanopores: A review and perspective. *J. Phys. Chem. C.* **123**, 21309–21326 (2019).
20. Wijmans, J. G. & Baker, R. W. The solution-diffusion model: a review. *J. Memb. Sci.* **107**, 1–21 (1995).
21. Mukherjee, P. & Sengupta, A. K. Ion exchange selectivity as a surrogate indicator of relative permeability of ions in reverse osmosis processes. *Environ. Sci. Technol.* **37**, 1432–1440 (2003).
22. Epsztein, R., Cheng, W., Shaulsky, E., Dizge, N. & Elimelech, M. Elucidating the mechanisms underlying the difference between chloride and nitrate rejection in nanofiltration. *J. Memb. Sci.* **548**, 694–701 (2017).
23. Sata, T. Studies on anion exchange membranes having permselectivity for specific anions in electrodialysis - Effect of hydrophilicity of anion exchange membranes on permselectivity of anions. *J. Memb. Sci.* **167**, 1–31 (2000).
24. Cheng, W. et al. Selective removal of divalent cations by polyelectrolyte multilayer nanofiltration membrane: Role of polyelectrolyte charge, ion size, and ionic strength. *J. Memb. Sci.* **559**, 98–106 (2018).
25. Collins, F. C. Activation energy of the Eyring theory of liquid viscosity and diffusion. *J. Chem. Phys.* **26**, 398–400 (1957).
26. Eyring, H. Viscosity, plasticity, and diffusion as examples of absolute reaction rates. *J. Chem. Phys.* **4**, 283–291 (1936).
27. Ewell, R. H. & Eyring, H. Theory of the viscosity of liquids as a function of temperature and pressure. *J. Chem. Phys.* **5**, 726–736 (1937).
28. Zwolinski, B. J., Eyring, H. & Reese, C. E. Diffusion and membrane permeability. *J. Phys. Colloid Chem.* **53**, 1426–1453 (1949).
29. Castillo, L. F. Del, Mason, E. A. & Viehland, L. A. Energy-barrier models for membrane transport. *Biophys. Chem.* **9**, 111–120 (1979).
30. Sogami, M. et al. Application of the transition state theory to water transport across cell membranes. *Biochim. Biophys. Acta - Biomembr.* **1511**, 42–48 (2001).
31. Babu, J. S. & Sathian, S. P. Combining molecular dynamics simulation and transition state theory to evaluate solid-liquid interfacial friction in carbon nanotube membranes. *Phys. Rev. E* **85**, 051205 (2012).
32. Epsztein, R., Qin, M., Shaulsky, E. & Elimelech, M. Activation behavior for ion permeation in ion-exchange membranes: Role of ion dehydration in selective transport. *J. Memb. Sci.* **580**, 316–326 (2019).
33. Latorre, R. & Miller, C. Conduction and selectivity in potassium channels. *J. Membr. Biol.* **71**, 11–30 (1983).
34. Wang, J. H., Robinson, C. V. & Edelman, I. S. Self-diffusion and structure of liquid water. III. Measurement of the self-diffusion of liquid water with H^2, H^3 and O^{18} as tracers. *J. Am. Chem. Soc.* **75**, 466–470 (1953).
35. Venkataraman, L., Klare, J. E., Nuckolls, C., Hybertsen, M. S. & Steigerwald, M. L. Dependence of single-molecule junction conductance on molecular conformation. *Nature* **442**, 904–907 (2006).
36. Pati, R. & Karna, S. P. Current switching by conformational change in a π-σ-π molecular wire. *Phys. Rev. B - Condens. Matter Mater. Phys.* **69**, 155419 (2004).
37. Weigelt, S. et al. Chiral switching by spontaneous conformational change in adsorbed organic molecules. *Nat. Mater.* **5**, 112–117 (2006).
38. Daasbjerg, K. et al. Evidence for large inner reorganization energies in the reduction of diaryl disulfides: Toward a mechanistic link between concerted and stepwise dissociative electron transfers? *J. Am. Chem. Soc.* **121**, 1750–1751 (1999).
39. Pophristic, V., Goodman, L. & Guchhait, N. Role of lone-pairs in internal rotation barriers. *J. Phys. Chem. A* **101**, 4290–4297 (1997).
40. Sharma, R. R., Agrawal, R. & Chellam, S. Temperature effects on sieving characteristics of thin-film composite nanofiltration membranes: Pore size distributions and transport parameters. *J. Memb. Sci.* **223**, 69–87 (2003).
41. Luo, J. & Wan, Y. Effects of pH and salt on nanofiltration-a critical review. *J. Membr. Sci.* **438**, 18–28 (2013).
42. Nghiem, L. D., Schäfer, A. I. & Elimelech, M. Role of electrostatic interactions in the retention of pharmaceutically active contaminants by a loose nanofiltration membrane. *J. Memb. Sci.* **286**, 52–59 (2006).
43. Epsztein, R., Shaulsky, E., Dizge, N., Warsinger, D. M. & Elimelech, M. Role of ionic charge density in Donnan exclusion of monovalent anions by nanofiltration. *Environ. Sci. Technol.* **52**, 4108–4116 (2018).
44. Richards, L. A., Schäfer, A. I., Richards, B. S. & Corry, B. The importance of dehydration in determining ion transport in narrow pores. *Small* **8**, 1701–1709 (2012).
45. Marcus, Y. Thermodynamics of solvation of ions. *J. Chem. Soc. Faraday Trans.* **87**, 2995–2999 (1991).
46. Ben-Amotz, D., Raineri, F. O. & Stell, G. Solvation thermodynamics: Theory and applications. *J. Phys. Chem. B* **109**, 6866–6878 (2005).
47. Sahu, S., Di Ventra, M. & Zwolak, M. Dehydration as a universal mechanism for ion selectivity in graphene and other atomically thin pores. *Nano Lett.* **17**, 4719–4724 (2017).
48. Richards, L. A., Schäfer, A. I., Richards, B. S. & Corry, B. Quantifying barriers to monovalent anion transport in narrow non-polar pores. *Phys. Chem. Chem. Phys.* **14**, 11633–11638 (2012).
49. Zwolak, M., Wilson, J. & Di Ventra, M. Dehydration and ionic conductance quantization in nanopores. *J. Phys. Condens. Matter* **22**, 454126 (2010).
50. Tansel, B. Significance of thermodynamic and physical characteristics on permeation of ions during membrane separation: Hydrated radius, hydration free energy and viscous effects. *Sep. Purif. Technol.* **86**, 119–126 (2012).

51. Sata, T., Yamaguchi, T. & Matsusaki, K. Effect of hydrophobicity of ion exchange groups of anion exchange membranes on permselectivity between two anions. *J. Phys. Chem.* **99**, 12875–12882 (1995).
52. Hannesschlaeger, C., Horner, A. & Pohl, P. Intrinsic membrane permeability to small molecules. *Chem. Rev.* **119**, 5922–5953 (2019).
53. De Gier, J., Mandersloot, J. G., Hupkes, J. V., McElhaney, R. N. & van Veek, W. P. On the mechanism of non-electrolyte permeation through lipid bilayers and through biomembranes. *Biochim. Biophys. Acta* **233**, 610–618 (1971).
54. Noy, A. Kinetic model of gas transport in carbon nanotube channels. *J. Phys. Chem. C.* **117**, 7656–7660 (2013).
55. Boo, C. et al. High performance nanofiltration membrane for effective removal of perfluoroalkyl substances at high water recovery. *Environ. Sci. Technol.* **52**, 7279–7288 (2018).
56. DuChanois, R. M., Epsztein, R., Trivedi, J. A. & Elimelech, M. Controlling pore structure of polyelectrolyte multilayer nanofiltration membranes by tuning polyelectrolyte-salt interactions. *J. Memb. Sci.* **581**, 413–420 (2019).
57. Farrokhzad, H., Darvishmanesh, S., Genduso, G., Van Gerven, T. & Van Der Bruggen, B. Development of bivalent cation selective ion exchange membranes by varying molecular weight of polyaniline. *Electrochim. Acta* **158**, 64–72 (2015).
58. Vaselbehagh, M., Karkhanechi, H., Takagi, R. & Matsuyama, H. Surface modification of an anion exchange membrane to improve the selectivity for monovalent anions in electrodialysis - experimental verification of theoretical predictions. *J. Memb. Sci.* **490**, 301–310 (2015).
59. Epsztein, R., Nir, O., Lahav, O. & Green, M. Selective nitrate removal from groundwater using a hybrid nanofiltration–reverse osmosis filtration scheme. *Chem. Eng. J.* **279**, 372–378 (2015).
60. Zhou, Y. & MacKinnon, R. The occupancy of ions in the K+ selectivity filter: Charge balance and coupling of ion binding to a protein conformational change underlie high conduction rates. *J. Mol. Biol.* **333**, 965–975 (2003).
61. Doyle, D. A. et al. The structure of the potassium channel: molecular basis of K+ conduction and selectivity. *Science* **280**, 69–77 (1998).
62. Morais-Cabral, Ä. H., Kaufman, A. & Mackinnon, R. Chemistry of ion coordination and hydration revealed by a K^+ channel-Fab complex at 2.0 Å resolution. *Nature* **414**, 43–48 (2001).
63. Gouaux, E. & MacKinnon, R. Principles of selective ion transport in channels and pumps. *Science* **310**, 1461–1465 (2005).
64. Barboiu, M. Encapsulation versus self-aggregation toward highly selective artificial K^+ channels. *Acc. Chem. Res.* **51**, 2711–2718 (2018).
65. Gilles, A. & Barboiu, M. Highly selective artificial K+ channels: An example of selectivity-induced transmembrane potential. *J. Am. Chem. Soc.* **138**, 426–432 (2016).
66. Glasstone, S., Laidler, K. J. & Eyring, H. *The Theory of Rate Processes* (McGraw-Hill Book Company, 1941).
67. Eyring, H. The activated complex and the absolute rate of chemical reactions. *Chem. Rev.* **17**, 65–77 (1935).
68. Kopec, W. et al. Direct knock-on of desolvated ions governs strict ion selectivity in K^+ channels. *Nat. Chem.* **10**, 813–820 (2018).
69. Schoch, R. B., Han, J. & Renaud, P. Transport phenomena in nanofluidics. *Rev. Mod. Phys.* **80**, 839–883 (2008).
70. Abraham, J. et al. Tunable sieving of ions using graphene oxide membranes. *Nat. Nanotechnol.* **12**, 546–550 (2017).
71. Li, W., Wu, W. & Li, Z. Controlling interlayer spacing of graphene oxide membranes by external pressure regulation. *ACS Nano* **12**, 9309–9317 (2018).
72. Simon, G. P. et al. Ion transport in complex layered graphene-based membranes with tuneable interlayer spacing. *Sci. Adv.* **2**, e1501272 (2016).
73. Chen, L. et al. Ion sieving in graphene oxide membranes via cationic control of interlayer spacing. *Nature* **550**, 1–4 (2017).
74. Joshi, R. K. et al. Precise and ultrafast molecular sieving through graphene oxide membranes. *Science* **343**, 752–754 (2014).
75. Choi, W. et al. Diameter-dependent ion transport through the interior of isolated single-walled carbon nanotubes. *Nat. Commun.* **4**, 2397 (2013).
76. Tunuguntla, R. H. et al. Enhanced water permeability and tunable ion selectivity in subnanometer carbon nanotube porins. *Science* **357**, 792–796 (2017).
77. Ali, S., Rehman, S. A. U., Luan, H. Y., Farid, M. U. & Huang, H. Challenges and opportunities in functional carbon nanotubes for membrane-based water treatment and desalination. *Sci. Total Environ.* **646**, 1126–1139 (2019).
78. Li, F., Li, L., Liao, X. & Wang, Y. Precise pore size tuning and surface modifications of polymeric membranes using the atomic layer deposition technique. *J. Memb. Sci.* **385–386**, 1–9 (2011).
79. Chen, P. et al. Atomic layer deposition to fine-tune the surface properties and diameters of fabricated nanopores. *Nano Lett.* **4**, 1333–1337 (2004).
80. Spichiger-keller, U. E. Ionophores, ligands and reactands. *Anal. Chim. Acta* **400**, 65–72 (1999).
81. Ovchinnikov, Y. A. Physico-chemical basis of ion transport through biological membranes: ionophores and ion channels. *Eur. J. Biochem.* **94**, 321–336 (1979).
82. Ammann, D. et al. Preparation of neutral ionophores for alkali and alkaline earth metal cations and their application in ion selective membrane electrodes. *Helv. Chem. Acta* **58**, 1535–1548 (1975).
83. Bowman-James, K. Alfred Werner revisited: The coordination chemistry of anions. *Acc. Chem. Res.* **38**, 671–678 (2005).
84. Kang, S. O., Begum, R. A. & Bowman-James, K. Amide-based ligands for anion coordination. *Angew. Chem. Int. Ed.* **45**, 7882–7894 (2006).
85. Prets, E., Badertscher, M., Welti, M., Morf, W. E. & Simon, W. Design features of ionophores for ion selective electrodes. *Pure Appl. Chem.* **60**, 567–574 (1988).
86. Almeida, M. I. G. S., Cattrall, R. W. & Kolev, S. D. Recent trends in extraction and transport of metal ions using polymer inclusion membranes (PIMs). *J. Memb. Sci.* **415–416**, 9–23 (2012).
87. Sheng, C., Wijeratne, S., Cheng, C., Baker, G. L. & Bruening, M. L. Facilitated ion transport through polyelectrolyte multilayer films containing metal-binding ligands. *J. Memb. Sci.* **459**, 169–176 (2014).
88. Toutianoush, A., El-Hashani, A., Schnepf, J. & Tieke, B. Multilayer membranes of *p*-sulfonato-calix[8]arene and polyvinylamine and their use for selective enrichment of rare earth metal ions. *Appl. Surf. Sci.* **246**, 430–436 (2005).
89. Acar, E. T., Buchsbaum, S. F., Combs, C., Fornasiero, F. & Siwy, Z. S. Biomimetic potassium-selective nanopores. *Sci. Adv.* **5**, eaav2568 (2019).
90. Fang, A., Kroenlein, K., Riccardi, D. & Smolyanitsky, A. Highly mechanosensitive ion channels from graphene-embedded crown ethers. *Nat. Mater.* **18**, 76–81 (2019).
91. Richards, L. A., Richards, B. S., Corry, B. & Schäfer, A. I. Experimental energy barriers to anions transporting through nanofiltration membranes. *Environ. Sci. Technol.* **47**, 1968–1976 (2013).
92. Sigurdardottir, S. B., DuChanois, R. M., Epsztein, R., Pinelo, M. & Elimelech, M. Energy barriers to anion transport in nanofiltration membranes: role of intra-pore diffusion. *J. Memb. Sci.* **603**, 117921 (2020).
93. Khavrutskii, I. V., Gorfe, A. A., Lu, B. & McCammon, J. A. Free energy for the permeation of Na+ and CI- ions and their Ion-pair through a zwitterionic dimyristoyl phosphatidylcholine lipid bilayer by umbrella integration with harmonic fourier beads. *J. Am. Chem. Soc.* **131**, 1706–1716 (2009).
94. Gao, P., Hunter, A., Summe, M. J. & Phillip, W. A. A method for the efficient fabrication of multifunctional mosaic membranes by inkjet printing. *ACS Appl. Mater. Interfaces* **8**, 19772–19779 (2016).
95. Rajesh, S., Yan, Y., Chang, H. C., Gao, H. & Phillip, W. A. Mixed mosaic membranes prepared by layer-by-layer assembly for ionic separations. *ACS Nano* **8**, 12338–12345 (2014).
96. Malmir, H. et al. Induced charge anisotropy: A hidden variable affecting ion transport through membranes. *Matter* **2**, 735–750 (2019).
97. Haji-Akbari, A. Forward-flux sampling with jumpy order parameters. *J. Chem. Phys.* **149**, 072303 (2018).
98. Tu, K. L., Nghiem, L. D. & Chivas, A. R. Coupling effects of feed solution pH and ionic strength on the rejection of boron by NF/RO membranes. *Chem. Eng. J.* **168**, 700–706 (2011).
99. Somrani, A., Hamzaoui, A. H. & Pontie, M. Study on lithium separation from salt lake brines by nanofiltration (NF) and low pressure reverse osmosis (LPRO). *Desalination* **317**, 184–192 (2013).
100. Saraf, A., Johnson, K. & Lind, M. L. Poly(vinyl) alcohol coating of the support layer of reverse osmosis membranes to enhance performance in forward osmosis. *Desalination* **333**, 1–9 (2014).
101. Nicolini, J. V., Borges, C. P. & Ferraz, H. C. Selective rejection of ions and correlation with surface properties of nanofiltration membranes. *Sep. Purif. Technol.* **171**, 238–247 (2016).
102. Qi, S. et al. Polymersomes-based high-performance reverse osmosis membrane for desalination. *J. Memb. Sci.* **555**, 177–184 (2018).
103. Richards, L. A., Vuachère, M. & Schäfer, A. I. Impact of pH on the removal of fluoride, nitrate and boron by nanofiltration/reverse osmosis. *Desalination* **261**, 331–337 (2010).
104. Jeong, B. H. et al. Interfacial polymerization of thin film nanocomposites: A new concept for reverse osmosis membranes. *J. Memb. Sci.* **294**, 1–7 (2007).
105. Hong, S. U., Malaisamy, R. & Bruening, M. L. Optimization of flux and selectivity in Cl-/SO42- separations with multilayer polyelectrolyte membranes. *J. Membr. Sci.* **283**, 366–372 (2006).
106. Mukherjee, D., Kulkarni, A. & Gill, W. N. Flux enhancement of reverse osmosis membranes by chemical surface modification. *J. Memb. Sci.* **97**, 231–249 (1994).
107. Harrison, C. J., Le Gouellec, Y. A., Cheng, R. C. & Childress, A. E. Bench-scale testing of nanofiltration for seawater desalination. *J. Environ. Eng.* **133**, 1004–1014 (2007).
108. Giagnorio, M. et al. Achieving low concentrations of chromium in drinking water by nanofiltration: membrane performance and selection. *Environ. Sci. Pollut. Res.* **25**, 25294–25305 (2018).

109. Redondo, J. A. & Frank, K. F. Sea water applications with FILMTEC reverse osmosis membranes from small to large plants in 10 years. *Desalination* **82**, 31–49 (1991).
110. Arena, J. T., McCloskey, B., Freeman, B. D. & McCutcheon, J. R. Surface modification of thin film composite membrane support layers with polydopamine: Enabling use of reverse osmosis membranes in pressure retarded osmosis. *J. Memb. Sci.* **375**, 55–62 (2011).
111. Al-Zoubi, H., Hilal, N., Darwish, N. A. & Mohammad, A. W. Rejection and modelling of sulphate and potassium salts by nanofiltration membranes: neural network and Spiegler-Kedem model. *Desalination* **206**, 42–60 (2007).
112. Widjaya, A., Hoang, T., Stevens, G. W. & Kentish, S. E. A comparison of commercial reverse osmosis membrane characteristics and performance under alginate fouling conditions. *Sep. Purif. Technol.* **89**, 270–281 (2012).
113. Malaisamy, R., Talla-Nwafo, A. & Jones, K. L. Polyelectrolyte modification of nanofiltration membrane for selective removal of monovalent anions. *Sep. Purif. Technol.* **77**, 367–374 (2011).
114. Wang, K. Y., Chung, T. S. & Qin, J. J. Polybenzimidazole (PBI) nanofiltration hollow fiber membranes applied in forward osmosis process. *J. Memb. Sci.* **300**, 6–12 (2007).
115. Freger, V., Arnot, T. C. & Howell, J. A. Separation of concentrated organic/inorganic salt mixtures by nanofiltration. *J. Memb. Sci.* **178**, 185–193 (2000).
116. Nilsson, M., Trägårdh, G. & Östergren, K. The influence of sodium chloride on mass transfer in a polyamide nanofiltration membrane at elevated temperatures. *J. Memb. Sci.* **280**, 928–936 (2006).
117. Tsuru, T., Izumi, S., Yoshioka, T. & Asaeda, M. Temperature effect on transport performance by inorganic nanofiltration membranes. *AIChE J.* **46**, 565–574 (2000).
118. Tsuru, T., Ogawa, K., Kanezashi, M. & Yoshioka, T. Permeation characteristics of electrolytes and neutral solutes through titania nanofiltration membranes at high temperatures. *Langmuir* **26**, 10897–10905 (2010).
119. Sharma, R. R. & Chellam, S. Temperature and concentration effects on electrolyte transport across porous thin-film composite nanofiltration membranes: Pore transport mechanisms and energetics of permeation. *J. Colloid Interface Sci.* **298**, 327–340 (2006).
120. Snow, M. J. H., de Winter, D., Buckingham, R., Campbell, J. & Wagner, J. New techniques for extreme conditions: high temperature reverse osmosis and nanofiltration. *Desalination* **105**, 57–61 (1996).
121. Saltonstall, C. W. Jr Practical aspects of sea water desalination by reverse osmosis. *Desalination* **18**, 315–320 (1976).
122. Li, L., Dong, J. & Nenoff, T. M. Transport of water and alkali metal ions through MFI zeolite membranes during reverse osmosis. *Sep. Purif. Technol.* **53**, 42–48 (2007).
123. Mehdizadeh, H., Dickson, J. M. & Eriksson, P. K. Temperature effects on the performance of thin-film composite, aromatic polyamide membranes. *Ind. Eng. Chem. Res.* **28**, 814–824 (1989).
124. Connell, P. J. & Dickson, J. M. Modeling reverse osmosis separations with strong solute-membrane affinity at different temperatures using the finely porous model. *J. Appl. Polym. Sci.* **35**, 1129–1148 (1988).
125. Chen, J.-Y., Nomura, H. & Pusch, W. Temperature dependence of membrane transport parameters in hyperfiltration. *Desalination* **46**, 437–446 (1983).
126. Lonsdale, H. K., Merten, U. & Riley, R. L. Transport properties of cellulose acetate osmotic membranes. *J. Appl. Polym. Sci.* **9**, 1341–1362 (1965).
127. Reid, C. E. & Kuppers, J. R. Physical characteristics of osmotic membranes of organic polymers. *J. Appl. Polym. Sci.* **2**, 264–272 (1959).
128. Gary-Bobo, C. M. Effect of geometrical and chemical constraints on water flux across artificial membranes. *J. Gen. Physiol.* **57**, 610–622 (2004).
129. Gary-Bobo, C. M. Role of hydrogen-bonding in nonelectrolyte diffusion through dense artificial membranes. *J. Gen. Physiol.* **54**, 369–382 (2004).
130. Badessa, T. & Shaposhnik, V. The electrodialysis of electrolyte solutions of multi-charged cations. *J. Memb. Sci.* **498**, 86–93 (2016).
131. Freger, V. et al. Diffusion of water and ethanol in ion-exchange membranes: Limits of the geometric approach. *J. Memb. Sci.* **160**, 213–224 (1999).
132. Kumar, M., Grzelakowski, M., Zilles, J., Clark, M. & Meier, W. Highly permeable polymeric membranes based on the incorporation of the functional water channel protein Aquaporin Z. *Proc. Natl Acad. Sci. USA* **104**, 20719–20724 (2007).
133. Borgnia, M. J., Kozono, D., Calamita, G., Maloney, P. C. & Agre, P. Functional reconstitution and characterization of AqpZ, the E. coli water channel protein. *J. Mol. Biol.* **291**, 1169–1179 (1999).
134. Corry, B. Designing carbon nanotube membranes for efficient water desalination. *J. Phys. Chem. B* **112**, 1427–1434 (2008).
135. Song, C. & Corry, B. Intrinsic ion selectivity of narrow hydrophobic pores. *J. Phys. Chem. B* **113**, 7642–7649 (2009).
136. Williams, C. D. & Carbone, P. Selective removal of technetium from water using graphene oxide membranes. *Environ. Sci. Technol.* **50**, 3875–3881 (2016).
137. Sahu, S. & Zwolak, M. Ionic selectivity and filtration from fragmented dehydration in multilayer graphene nanopores. *Nanoscale* **9**, 11424–11428 (2017).
138. Konatham, D., Yu, J., Ho, T. A. & Striolo, A. Simulation insights for graphene-based water desalination membranes. *Langmuir* **29**, 11884–11897 (2013).
139. Zwolak, M., Lagerqvist, J. & Di Ventra, M. Quantized ionic conductance in nanopores. *Phys. Rev. Lett.* **103**, 128102 (2009).
140. Arrhenius, S. A. Über die Reaktionsgeschwindigkeit bei der Inversion von Rohrzucker durch Säuren. *Z. Phys. Chem.* **4**, 226–248 (1889).
141. Eyring, H. The theory of absolute reaction rates. *Trans. Faraday Soc.* **34**, 41–48 (1938).
142. Kramers, H. A. Brownian motion in a field of force and the diffusion model of chemical reactions. *Physica* **7**, 284–304 (1940).
143. Hanggi, P. 50 years after Kramers. *Rev. Mod. Phys.* **62**, 251–341 (1990).
144. Wynne-Jones, W. F. K. & Eyring, H. The absolute rate of reactions in condensed phases. *J. Chem. Phys.* **3**, 492–502 (1935).
145. Garrett, B. C. Variational transition state theory. *Ann. Rev. Phys. Chem.* **35**, 159–189 (1984).

Acknowledgements

This work was supported by the Center for Enhanced Nanofluidic Transport (CENT), an Energy Frontier Research Center funded by the US Department of Energy, Office of Science, Basic Energy Sciences under award no. DE-SC0019112.

Competing interests

The authors declare no competing interests.

Additional information

Correspondence should be addressed to M.E.

Reprints and permissions information is available at www.nature.com/reprints.

Publisher's note Springer Nature remains neutral with regard to jurisdictional claims in published maps and institutional affiliations.

© Springer Nature Limited 2020